

## **Chapter 7**

# **SINGLE CONTACT POINT TRANSIENT TYRE MODELS**

### **7.1. Introduction**

For relatively low frequency and large wavelength transient and oscillatory vehicle motions, tyre inertia and the effect of the finite length of the contact patch may be neglected or taken care of in an approximative manner. In Chapter 5 a thorough treatment has been given of the out-of-plane stretched string tyre model together with a number of approximate models. One of these models did ignore the contact length. For the aligning torque the effect of tread width and the gyroscopic couple were introduced.

The present chapter deals with the further development of this type of model which in its simplest form has been and still is very popular in vehicle dynamics studies. Both in-plane and out-of-plane models will be discussed for small slip, linear and for large slip, non-linear conditions. The concept of the relaxation length is central in the model structure. The development of the single point contact models follows an essentially different and much simpler line compared with the theoretical approach on which the string model is based. Because of its simplicity it is possible to enhance the model to cover the full non-linear combined slip range including rolling from standstill or even change direction from forwards to backwards rolling. Camber and turn slip may be included.

With the linear and non-linear models, to be developed in this chapter, various vehicle dynamics problems may be approximately analysed such as the shimmy phenomenon (cf. curve for single point model in Fig.6.2), transient vehicle motions with oscillatory steer inputs, motion over undulated road surfaces at side slip and camber, steering vibrations induced by wheel imbalance and tyre out-of-roundness. In these studies the effect of tyre lag may be ascertained. In a number of applications to be treated in Chapter 8 we will address these problems (except wheel shimmy, which was the subject of Chapter 6).



have been shown as negative quantities. The difference of the velocities of the two points cause the carcass springs to deflect. Consequently, the time rates of change of the longitudinal and lateral deflections  $u$  and  $v$  read:

$$\frac{du}{dt} = -(V_{sx} - V'_{sx}) \quad (7.1)$$

and

$$\frac{dv}{dt} = -(V_{sy} - V'_{sy}) \quad (7.2)$$

If we assume small values of slip we may write for the side force acting from road to contact patch with  $C_{Fa}$  denoting the cornering or side slip stiffness:

$$F_y = C_{Fa} \alpha' = -C_{Fa} \frac{V'_{sy}}{|V_x|} \quad (7.3)$$

It is assumed here that the difference between the wheel centre longitudinal velocity  $V_x$  and the longitudinal velocity  $V_{cx}$  of the contact centre is negligible.

$$V_{cx} \approx V_x \quad (7.4)$$

Consequently, we may employ  $V_x$  in the present chapter. With the lateral tyre stiffness at road level  $C_{Fy}$  we have for the elastic internal force that balances the side slip force:

$$F_y = C_{Fy} v \quad (7.5)$$

and we can write for Eq.(7.2) with (7.3,7.5) after having introduced the relaxation length for side slip  $\sigma_a$ :

$$\sigma_a = \frac{C_{Fa}}{C_{Fy}} \quad (7.6)$$

the differential equation for the lateral deflection due to side slip  $v_a$  (later on we will also have a lateral deflection due to camber):

$$\frac{dv_a}{dt} + \frac{1}{\sigma_a} |V_x| v_a = |V_x| \alpha = -V_{sy} \quad (7.7)$$

Where  $\alpha$  is the wheel slip angle:  $\alpha \approx -V_{sy}/|V_x|$ . The side force is obtained by multiplying  $v_a$  with  $C_{Fy}$ .

In a similar way we can deal with the longitudinal force response. With the longitudinal tyre stiffness  $C_{Fx}$  at road level and the longitudinal slip stiffness  $C_{Fk}$  we obtain for the relaxation length  $\sigma_k$ :

$$\sigma_k = \frac{C_{Fk}}{C_{Fx}} \quad (7.8)$$

and we can derive with Eq.(7.1) the differential equation for the fore and aft deflection  $u$

$$\frac{du}{dt} + \frac{1}{\sigma_\kappa} |V_x| u = |V_x| \kappa = -V_{sx} \quad (7.9)$$

with  $\kappa$  the longitudinal wheel slip ratio:  $\kappa \approx -V_{sx}/|V_x|$ . The longitudinal force may be obtained by multiplying  $u$  with the stiffness  $C_{Fx}$ .

Next, we consider wheel camber as input. For a suddenly applied camber angle  $\gamma$  (about the line of intersection at ground level!), we assume that a contact line curvature and thus the camber thrust  $C_{Fy}\gamma$  is immediately felt at the contact patch. As a reaction, a contact patch side slip angle  $\alpha'$  is developed that builds up the lateral carcass deflection  $v=v_\gamma$ . Again Eq.(7.5) applies. The side force that acts on the wheel now becomes:

$$F_y = C_{Fy} v_\gamma = C_{Fy} \gamma + C_{Fa} \alpha' \quad (7.10)$$

With wheel side slip kept equal to zero,  $V_{sy}=0$ , and  $V'_{sy} = -|V_x| \alpha'$  Eq.(7.2) can be written in the form:

$$\frac{dv_\gamma}{dt} + \frac{1}{\sigma_a} |V_x| v_\gamma = \frac{C_{Fy}}{C_{Fa}} |V_x| \gamma \quad (7.11)$$

This equation shows that according to this simple model the camber force relaxation length  $\sigma_\gamma$  is equal to the relaxation length for side slip  $\sigma_a$ . This theoretical result is substantiated by careful step response experiments, performed by Higuchi (1997) on a flat plank test rig (cf. Sec.7.2.3).

A similar equation results for the total spin  $\varphi$  including turn slip and camber:

$$\frac{dv_\varphi}{dt} + \frac{1}{\sigma_a} |V_x| v_\varphi = \frac{C_{F\varphi}}{C_{Fa}} |V_x| \varphi \quad (7.12)$$

with according to Eq.(4.76):

$$\varphi = -\frac{1}{V_x} \{ \dot{\psi} - (1 - \varepsilon_\gamma) \Omega \sin \gamma \} \quad (7.13)$$

that shows that the turn slip velocity  $\dot{\psi}$  can be converted into an equivalent camber angle.

The forces and moment are obtained from the deflections  $u$  and  $v$  by first assessing the transient slip quantities  $\alpha'$ ,  $\kappa'$  and  $\gamma'$  and from these with the slip stiffnesses the forces and moment.

According to the adopted steady-state model, Eq.(4.E71), the moment response to camber (and turn slip) is the sum of the residual torque,  $M_{zr}$ , assumedly mainly due to finite tread width, and  $-t_\alpha F_y$ , assumedly caused by camber induced side slip, cf. discussion later on (below Eq.(7.40)). A first-order

approximation for the response of  $M_{zr}$  with the short relaxation length equal to half the contact length  $a$  may be employed. This, however, will be saved for Chapter 9 where short wavelengths responses are considered. Here we suffice with the assumption that the moment due to tread width responds instantaneously to camber and turn slip.

For the linear, small slip condition we find:

$$\alpha' \approx \tan \alpha' = \frac{v_a}{\sigma_a}, \quad F_{ya} = C_{Fa} \alpha', \quad M_{za} = -C_{Ma} \alpha' = -t_a F_{ya} \quad (7.14)$$

$$\kappa' = \frac{u}{\sigma_\kappa}, \quad F_x = C_{F\kappa} \kappa' \quad (7.15)$$

$$\gamma' = \frac{C_{Fa}}{C_{F\gamma}} \frac{v_\gamma}{\sigma_a}, \quad F_{y\gamma} = C_{F\gamma} \gamma', \quad M_{z\gamma} = (C_{M\gamma} + t_a C_{F\gamma}) \gamma \quad (7.16)$$

and similar for  $\varphi$ . The pneumatic trail due to side slip is denoted here with  $t_a$ . The total aligning torque becomes (cf. Eq.(4.E71) and Fig.4.21):

$$M_z = -t_a (F_{ya} + F_{y\gamma}) + M_{z\gamma} \quad (7.17)$$

In an alternative model, used for motorcycle dynamics studies, the terms with  $t_a C_{F\gamma}$  or  $t_a F_{y\gamma}$  in (7.16,7.17) are omitted, cf. discussion below Eq.(7.40).

The equations (7.7,7.9,7.11) may be written in terms of the transient slip quantities. For example, we may express  $v_a$  in terms of  $\alpha'$  by using the first equation of (7.14). Insertion in (7.7) gives:

$$\sigma_a \frac{d\alpha'}{dt} + |V_x| \alpha' = |V_x| \alpha = -V_{sy} \quad (7.18)$$

If we recognise the fact that the relaxation length is a function of the vertical load and if the average slip angle is unequal to zero, an additional term shows up in the linearised equation (variation of  $\alpha'$  and of  $F_z(t)$  are small!) which results from the differentiation of  $v_a = \sigma_a \alpha'$  with respect to time. Then, Eq.(7.7) becomes:

$$\sigma_a \frac{d\alpha'}{dt} + \left( |V_x| + \frac{d\sigma_a}{dF_z} \frac{dF_z}{dt} \right) \alpha' = |V_x| \alpha = -V_{sy} \quad (7.19)$$

Obviously, when using Eq.(7.18) a response to a variation of the vertical load can not be expected. If the load varies, Eq.(7.18) is inadequate and the original equation (7.7) should be used or the corresponding equation (7.19).

With (7.5) equation (7.7) may be written directly in terms of  $F_y$ . If we may consider the carcass lateral stiffness  $C_{Fy}$  virtually independent of the wheel load  $F_z$  we obtain by using Eq.(7.6) :

$$\sigma_a \frac{dF_y}{dt} + |V_x| F_y = |V_x| F_{yss} \quad (7.20)$$

Since we have the same relaxation length for both the responses to side slip and

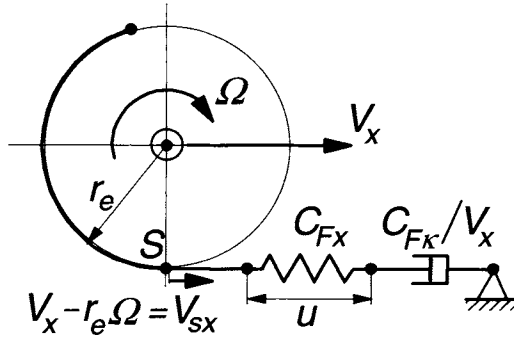


Fig. 7.2. Mechanical model of transient tangential tyre behaviour.

camber, this equation appears to hold for the combined linear response to the inputs  $\alpha$  and  $\gamma$  or  $\varphi$ . In the right-hand member  $F_{yss}$  denotes the steady-state (instantaneous) response to these inputs and possibly a changing vertical load at a given slip condition. Multiplication with the pneumatic trail produces the moment  $-M'_z$  (if  $\gamma = \varphi = 0$ ). A similar differential equation may be written for the  $F_x$  response to  $\kappa$ .

The equations (7.7,7.9) have been written in the form ( $V_x$  not in denominator and  $V_{sx,y}$  used as right-hand member) that makes them applicable for simulations of stopping and starting from zero speed occurrences. At speed  $V_x = 0$  Eq.(7.9) turns into an integrator:  $u = -\int V_{sx} dt$ . With Eq.(7.15) the longitudinal force becomes:  $F_x = C_{Fx} K' = C_{Fx} u / \sigma_\kappa$  which with (7.8) is equal to:  $C_{Fx} u$ . This is the correct expression for the tyre that at standstill acts like a longitudinal or tangential spring. When the wheel starts rolling, the tyre gradually changes into a damper with rate:  $C_{Fx} / |V_x|$ . Figure 7.2 depicts a corresponding mechanical model with spring and damper in series. It shows that at low speed the damper becomes very stiff and the spring dominates. At higher forward velocities the spring becomes relatively stiff and the damper part dominates the behaviour of the tyre. A similar model may be drawn for the transient lateral behaviour. It may be noted that the equation (7.20) is not suited for moving near or at  $V_x = 0$ . In Section 8.6 the use of the transient models for the response to lateral and longitudinal wheel slip speed at and near zero speed will be demonstrated.

Apparently, Eq.(7.12) with (7.13) fails to describe the response to variations in wheel yaw angle  $\psi$  at vanishing speed. Then, the lateral deflection becomes  $v_\varphi = -(C_{F\varphi}/C_{F\alpha}) \int d\psi$ . With  $\varphi' = (C_{F\alpha}/C_{F\varphi}) v_\varphi / \sigma_\alpha$  we have  $\varphi' = -\psi / \sigma_\alpha$  indicating an instantaneous response of  $F_y$  which, however, should remain zero! We refer to Chapter 9, Section 9.2.1, Eq.(9.56 etc.), that suggests a further developed model that can handle this situation correctly. Consequently, it must be concluded that the present transient model cannot be employed to simulate parking manoeuvres unless  $F_y$  is suppressed artificially in the lower speed range.

### 7.2.2. Semi-Non-Linear Model

For the extension of the linear theory to cover the non-linear range of the slip characteristics, it may be tempting to employ Eq.(7.20) and use the instantaneous non-linear force response as input in the differential equation. The input steady-state side force is calculated, e.g. with the *Magic Formula*, using the current wheel slip angle  $\alpha$ . This method, however, may lead to incorrect results as due to the phase lag in side force response, the current (varying) wheel load may not correspond to the calculated magnitude attained by the side force. In limit conditions the tyre may then be predicted to be still in adhesion while in reality full sliding occurs. A better approach is the utilisation of the original equation (7.7) and calculate the side force afterwards by using the resulting transient slip angle  $\alpha'$  as input in the *Magic Formula*.

In general, we have the three equations (7.7,7.9,7.11) and possibly (7.12) and the first equations of (7.14-16) producing  $\alpha'$ ,  $\kappa'$  and  $\gamma'$  or  $\varphi'$  which are used as input in the non-linear force and moment functions ( $\gamma$  or  $\varphi$  directly in the expressions for  $M_r$ ), e.g. the equations of the *Magic Formula* tyre model (Chapter 4).

$$F_x = F_x(\kappa', \alpha', F_z) \quad (7.21)$$

$$F_y = F_y(\alpha', \gamma', \kappa', F_z) \quad (7.22)$$

$$M'_z = -t_a F_y \quad (7.23)$$

$$M_{zr} = M_{zr}(\gamma, \alpha', \kappa', F_z) \quad (7.24)$$

$$M_z = M'_z + M_{zr} + s \cdot F_x \quad (4.E71)$$

where if required,  $\gamma$  may be replaced by  $\varphi$  as the spin argument.

This non-linear model is straightforward and is often used in transient or low frequency vehicle motion simulation applications. Starting from zero speed or stopping to standstill is possible. However, as has been mentioned before, at  $V_x$  equal or close to zero the equations (7.7,7.9) act as integrators of the slip speed components  $V_{sx,y}$ , which may give rise to possibly very large deflections. The limitation of these deflections may be accomplished by making the derivatives of the deflections  $u$  and  $v$  equal to zero, if (1) the forward wheel velocity has become very small ( $<V_{low}$ ) and (2) the deflections take values larger than physically possible. This can be seen to correspond with the combined equivalent side slip value exceeding the level  $\alpha_{sl}$  where the peak horizontal force occurs. Approximately, we may adopt the following limiting algorithm with the equivalent slip angle according to Eq.(4.E78):

$$\begin{aligned}
&\text{if: } |\alpha'_{r,eq}| > \alpha_{sl} \text{ and } |V_x| < V_{low} \\
&\text{then: } \text{if: } (V_{sx} + |V_x|u/\sigma_\kappa)u < 0 : \dot{u} = 0 \quad \text{else: Eq.(7.9) applies} \\
&\quad \text{if: } (V_{sy} + |V_x|v/\sigma_\alpha)v < 0 : \dot{v} = 0 \quad \text{else: Eq.(7.7) applies} \\
&\text{else: Eqs.(7.7,7.9) apply} \\
&\text{with roughly:} \\
&\quad \alpha_{sl} = 3D_y/C_{Fa}
\end{aligned} \tag{7.25}$$

Experience in applying the model has indicated that starting from standstill gives rise to oscillations which are practically undamped. Damping increases when speed is built up. To artificially introduce some damping at very low speed, which with the actual tyre is established through material damping, one might employ the following expression for the transient slip  $\kappa'$ , as suggested by Besselink, instead of Eq.(7.15):

$$\kappa' = \left( \frac{u}{\sigma_\kappa} - \frac{k_{Vlow}}{C_{F\kappa}} V_{sx} \right) \tag{7.26}$$

The damping coefficient  $k_{Vlow}$  should be gradually suppressed to zero when the speed of travel  $V_x$  approaches a selected low value  $V_{low}$ . Beyond that value the model should operate as usual. In Chapter 8, Sec.8.6 an application will be given. A similar equation may be employed for the lateral transient slip.

Another extreme situation is the condition at wheel lock. At steady state Eq.(7.9) reduces to:

$$\frac{1}{\sigma_\kappa} |V_x| u = -V_x \tag{7.27}$$

which indicates that the deflection  $u$  according to the semi-linear theory becomes as large as the relaxation length  $\sigma_\kappa$ . Avoiding the deflections from becoming too large, which is of importance at e.g. repetitive braking, calls for an enhanced non-linear model. Another shortcoming of the model that is to be tackled concerns the experimentally observed property of the tyre that its relaxation length depends on the level of slip. At higher levels of side slip, the tyre shows a quicker response to additional changes in side slip. This indicates that the relaxation lengths decrease with increasing slip.

### 7.2.3. Fully Non-Linear Model

Figure 5.29, repeated here as Fig.7.3 shows the deflected string model provided with tread elements at various levels of steady-state side slip. Clearly, this model predicts that the 'intersection' length  $\sigma^*$  decreases with increasing  $\alpha$  that is: when



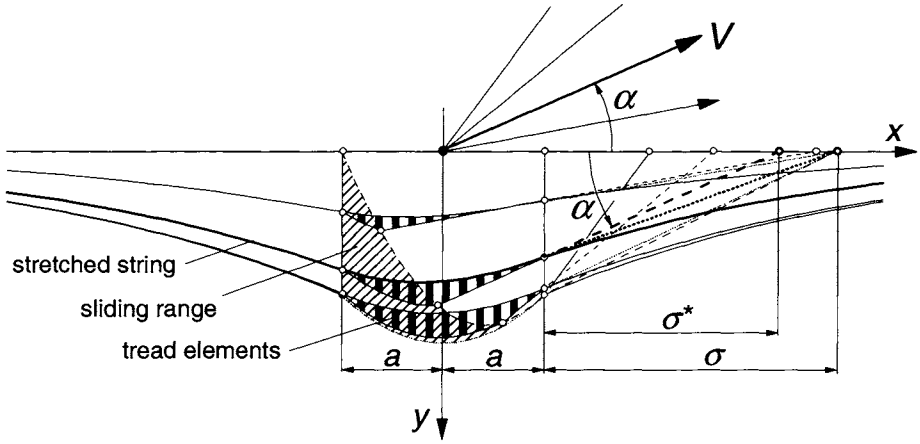


Fig. 7.3. The string tyre model with tread elements at increasing slip angles showing growing sliding range and decreasing 'intersection' length  $\sigma^*$ .

the sliding range grows. In the single point contact model we may introduce a similar reduction of the corresponding length. The intersection length  $\sigma_a^*$  is defined here as the ratio of the lateral deflection  $v_a$  and the transient lateral slip  $\tan \alpha'$ :

$$\sigma_a^* = \frac{v_a}{\tan \alpha'} \quad (7.28)$$

In Eq.(7.7) the relaxation length  $\sigma$  is replaced by  $\sigma^*$  and we get:

$$\frac{dv_a}{dt} + \frac{1}{\sigma_a^*} |V_x| v_a = |V_x| \tan \alpha = -V_{sy} \quad (7.29)$$

with apparently:

$$\sigma_a^* = \frac{1}{C_{Fy}} \frac{F_y}{\tan \alpha'} = \frac{\sigma_{ao}}{C_{Fa}} \frac{F_y}{\tan \alpha'} \approx \frac{\sigma_{ao}}{C_{Fa}} \frac{|F_y'| + C_{Fa} \varepsilon_F}{|\tan \alpha_f'| + \varepsilon_F} \quad (7.30)$$

with the initial relaxation length (at  $\alpha' = 0$ ):

$$\sigma_{ao} = \frac{C_{Fa}}{C_{Fy}} \quad (7.31)$$

to which  $\sigma_a^*$  approaches when  $\alpha' \rightarrow 0$ . To avoid singularity, one may use the last expression of (7.30) with small  $\varepsilon_F$  and add to  $\alpha'$  the shift  $\Delta \alpha$  to arrive at  $\alpha_f'$  as indicated in Fig.4.22. Figure 7.4 presents the characteristic of the intersection length together with the side force characteristic from which it is derived. Also in the equation for the camber deflection response (7.11) the relaxation length  $\sigma_a$

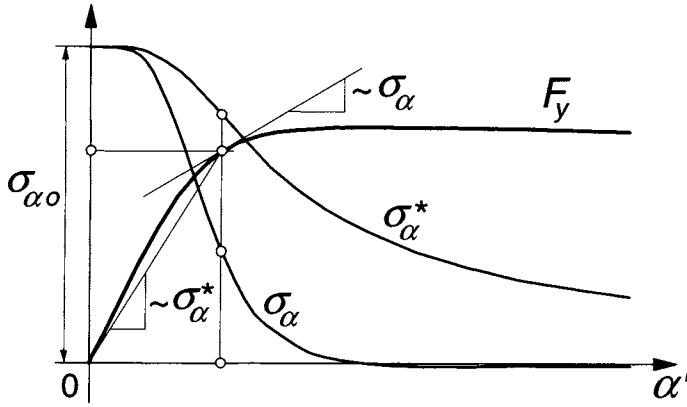


Fig. 7.4. Characteristics of tyre side force, 'intersection length'  $\sigma_\alpha^*$  and relaxation length  $\sigma_\alpha$ .

is replaced by  $\sigma_\alpha^*$ .

A more direct way to write Eq.(7.29) is yielded by eliminating  $\sigma_\alpha^*$  with the use of Eq.(7.28):

$$\frac{dv_\alpha}{dt} + |V_x| \tan \alpha' = |V_x| \tan \alpha = -V_{sy} \quad (7.32)$$

The transient slip angle  $\alpha'$  is obtained from the deflection  $v_\alpha$  by using the inverse possibly adapted  $F_y'(\alpha')$  characteristic, cf. Higuchi (1997):

$$v_\alpha = \frac{F_y'(\alpha')}{C_{Fy}} \quad (7.33)$$

To avoid double valued solutions a for this purpose adapted characteristic for  $F_y'(\alpha')$  in (7.30) or (7.33) may be required showing a positive slope in the slip range of interest. The value for  $\alpha'$  or for  $\sigma_\alpha^*$  when Eq.(7.29) is used, is obtained through iterations or by using information from the previous time step, cf. Higuchi(1997), Pacejka and Takahashi (1992), Takahashi and Hoshino (1996). The ultimate value of the force  $F_y$  is finally obtained from Eq.(7.22) by using the computed  $\tan \alpha' (= v_\alpha / \sigma_\alpha^*)$ .

Writing the equation (7.32) entirely in terms of the transient slip angle by using (7.5) with  $v = v_\alpha$  and remembering that  $F_y = F_y(\alpha', F_z)$  directly yields:

$$\frac{1}{C_{Fy}} \frac{\partial F_y}{\partial \tan \alpha'} \frac{d \tan \alpha'}{dt} + |V_x| \tan \alpha' = -V_{sy} - \frac{1}{C_{Fy}} \frac{\partial F_y}{\partial F_z} \frac{dF_z}{dt} \quad (7.34)$$

The additional input  $dF_z/dt$  requires information of the slope  $\partial F_y / \partial F_z$  at given values of the slip angle. If the vertical load remains constant the last term vanishes and we have the often used equation of the restricted fully non-linear model:

$$\sigma_\alpha \frac{d \tan \alpha'}{dt} + |V_x| \tan \alpha' = -V_{sy} \quad (7.35)$$

with

$$\sigma_\alpha = \frac{1}{C_{Fy}} \frac{\partial F_y}{\partial \tan \alpha'} \quad (7.36)$$

If we consider an average slip angle  $\alpha_0$  and a small variation  $\tilde{\alpha}$  of  $\tan \alpha$  and the corresponding lateral slip velocities, Eq.(7.35) becomes after having subtracted the average part:

$$\sigma_\alpha \frac{d \tilde{\alpha}'}{dt} + |V_x| \tilde{\alpha}' = -\tilde{V}_{sy} \quad (7.37)$$

which indicates that the structure of (7.35) is retained and that  $\sigma_\alpha$  (7.36) represents the actual relaxation length of the linearised system at a given load and slip angle. Its characteristic has been depicted in Fig.7.4 as well. Obviously, the relaxation length is associated with the slope of the side force characteristic. It also shows that the relaxation length becomes negative beyond the peak of the side force characteristic which makes the solution of (7.35) but also of the original equation (7.29) or (7.32) unstable if the point of operation lies in that range of side slip. We may, however, limit  $\sigma_\alpha$  downwards to avoid both instability and excessive computation time:  $\sigma_\alpha = \max(\sigma_\alpha, \sigma_{\min})$ . The transient response of the variation of the force proceeds in proportion with the variation of  $\tilde{\alpha}'$  as  $\tilde{F}_y = (\partial F_y / \partial \tan \alpha) \tilde{\alpha}'$ .

When the Eq.(7.35) is used, an algebraic loop does not occur as is the case when Eq.(7.29) is employed. The relaxation length  $\sigma_\alpha$  can be directly determined from the already available  $\tan \alpha'$ . However, since the last term of (7.34) has been omitted, equation (7.35) has become insensitive to  $F_z$  variations.

Similar functions and differential equations can be derived for the transient response to longitudinal slip. We obtain for the distance factors:

$$\sigma_\kappa^* = \frac{1}{C_{Fx}} \frac{F_x}{\kappa'} = \frac{\sigma_{\kappa 0}}{C_{F\kappa}} \frac{F_x}{\kappa'} \approx \frac{\sigma_{\kappa 0}}{C_{F\kappa}} \frac{|F_x| + C_{F\kappa} \varepsilon_F}{|\kappa'| + \varepsilon_F} \quad (7.38)$$

and

$$\sigma_\kappa = \frac{1}{C_{Fx}} \frac{\partial F_x}{\partial \kappa'} \quad (7.39)$$

It is of interest to note that the extreme case of wheel lock can now be handled correctly. As we have seen below Eq.(7.27), the deflection then becomes equal to minus the relaxation length which according to the fully non-linear model becomes:  $u = -\sigma_\kappa^*$ . With (7.38) and  $\kappa' = -1$  the deflection takes the value that

would actually occur at wheel lock:  $u = F_x / C_{Fx}$ .

The use of Eqs.(7.29,7.32) is attractive for simulation purposes because the solution contains the transient effect of changing vertical load. However, we may have computational difficulties to be reckoned with which may require some preparations. Using Eq.(7.35) proceeds in a straightforward manner if the derivative of the force vs slip characteristic is known beforehand. This requires some preparation and may become quite complex if the general combined slip situation is to be considered. Approximations using equivalent total slip according to Eq.(4.E78) may be realisable. A drawback, of course, is the fact that Eq.(7.35) does not respond to changes in  $F_z$ . In Chapter 9 this equation is used to handle the transient response of the tread deflections in the contact patch.

Figures 7.5-12 present results obtained by Higuchi (1997) for a passenger car 205/60R15 tyre tested on a flat plank machine (TU-Delft, cf. Fig.12.5). Figure 7.5 shows the response of the side force to step changes in slip angle at the nominal load of 4000N. The diagram clearly indicates the difference in behaviour at the different levels of side slip with a very rapid response occurring at  $\alpha = 10^\circ$ . The fully non-linear model according to Eqs.(7.32) or (7.29) or as in this case, with constant vertical load, Eq.(7.35), in conjunction with Eqs.(7.22,7.23) gives satisfactory agreement. The measured response curves have been corrected for the side force variation that arises already at zero slip angle. The test is performed by loading the tyre after the slip angle (steer angle) has been applied. Subsequently, the plank is moved. The aligning torque behaves in a similar manner although a little initial delay in response occurs as correctly predicted by the string model and shown in Fig.5.12. At larger slip angles (beyond the level where the  $M_z$  peak occurs) the aligning torque first shows a peak in the response after which the moment decays to its steady-state value. This behaviour is nicely followed by the model. Figure 7.6 shows the side force response to small increments in slip angle. The experiment is conducted by, after having stopped the plank motion, steering the wheel half a degree further and continue the forward motion. It was first ascertained that the response of the side force to a step steer input was hardly influenced by having first lifted the tyre from the road surface or not. Of course, the aligning moment response, in the latter case, is quite different because of initial torsion about the vertical axis. The resulting side force responses as depicted in Fig.7.6 have been compared with the exponential response of the side force increment as predicted by the solution of Eq.(7.37) with (7.36). Fitting with a least square procedure gave the relaxation length  $\sigma_a$  as presented in Fig.7.7. The resulting variation of  $\sigma_a$  with slip angle level is compared with the slope of the steady-state side force characteristic, both normalised making their values equal to unity at vanishing slip angle.

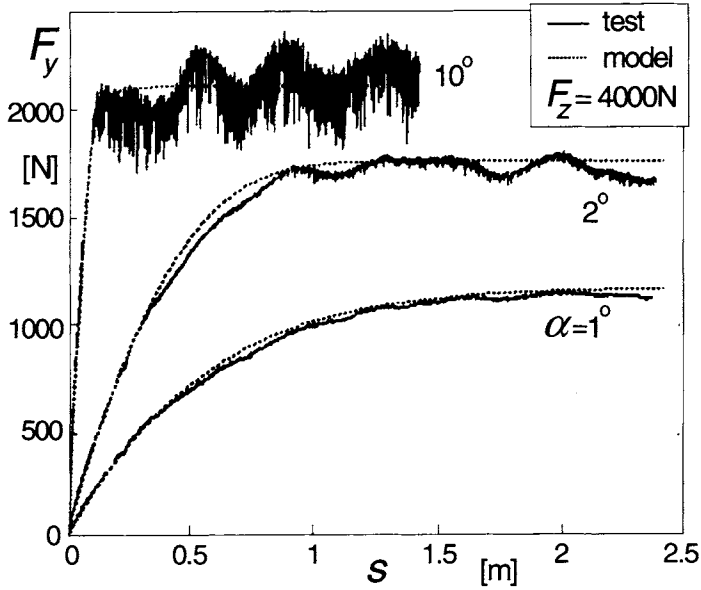


Fig. 7.5. Side force response to small and large step change in slip angle as assessed by flat plank experiments and computed with the model defined by Eqs.(7.32) or (7.29).

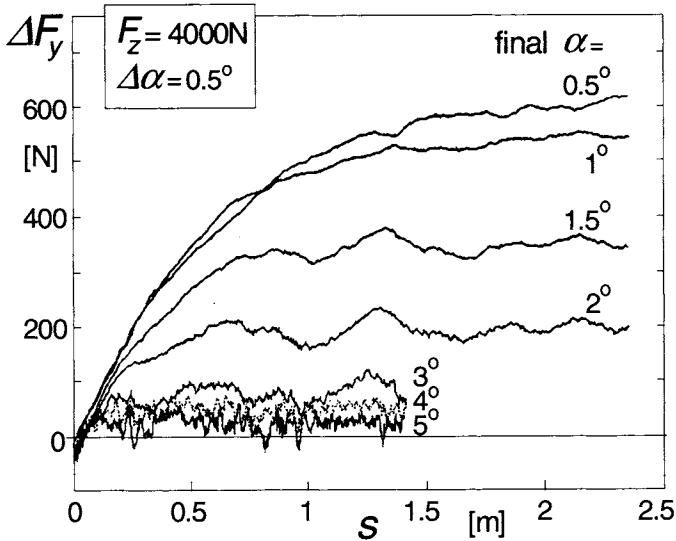


Fig. 7.6. Measured side force response to small increment of slip angle  $\Delta\alpha$  at different levels of slip angle indicating the decrease of relaxation length at increasing side slip level which is in agreement with expression (7.36).

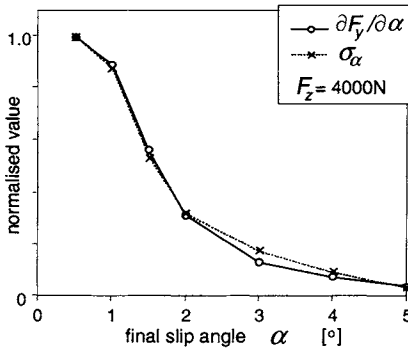


Fig. 7.7. Correspondence between  $F_y$  vs  $\alpha$  slope and relaxation length  $\sigma_\alpha$  as assessed by experiments.

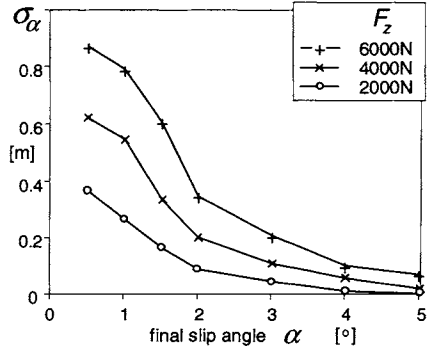


Fig. 7.8. Relaxation length measured at various wheel loads, decaying with increasing slip angle.

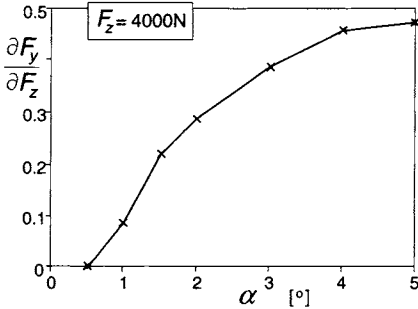


Fig. 7.9. The slope of  $F_y$  vs  $F_z$  as a function of slip angle, appearing in Eq.(7.34), as assessed by tests.

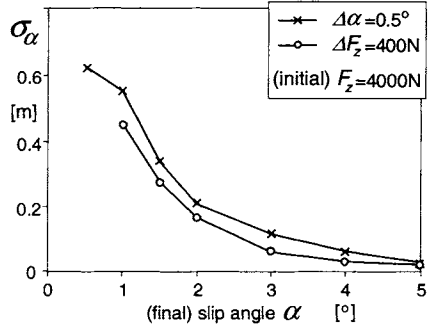


Fig. 7.10. Relaxation lengths resulting from small step changes in slip angle or wheel load, as function of slip angle level.

The excellent agreement supports the theoretical findings. Additional experiments have been conducted by Higuchi investigating the response to small increments in vertical load at constant slip angle. As shown by Eq.(7.34) the partial derivative  $\partial F_y / \partial F_z$  plays the role as input parameter. Figure 7.9 shows its variation with slip angle level. Figure 7.10 compares the resulting relaxation length values with those associated with changes in slip angle at constant load. Apparently, the relaxation length for slip angle change is larger than the one belonging to load change. However, due to the finite magnitude of the increments ( $0.5^\circ$  and 400N respectively) the actual differences are expected to be smaller. In the diagram, the curve for  $\Delta\alpha$  may be better shifted to the left over  $0.25^\circ$  while the curve for  $\Delta F_z$  may be reduced a little in height using information from Fig.7.8 accounting for a decrease of the average load level of 200N.

Higuchi also investigated the responses to changes in camber angle, and to

a limited extent also to the related turn slip. The change in camber was correctly established by rotating the road surface (the plank) about the line of intersection of wheel centre plane and plank surface (Fig.12.5, steer angle is kept equal to zero). The step response to turn slip  $\varphi_t = -1/R$  is obtained by integrating the response to a pulse change in turn slip, that is: load tyre, twist ( $\psi$ ) and then roll in the new wheel plane direction, and multiply the result with  $1/(R\psi)$ . The responses to camber and turn slip show quantitatively similar responses, cf. Pacejka (2004). The small initial delay of the response of the car tyre side force to camber and turn slip (cf. Figs.5.12,5.10) will effectively increase the relaxation length a little. Figures 7.11a and 7.11b show the responses of side force and moment to step changes in camber angle. The side force behaves in a manner similar to the response to side slip, Fig.7.5. Since we have a camber stiffness much smaller than the cornering stiffness, the camber force characteristic remains almost linear over a larger range of the camber angle (meaning: there is less sliding in the contact patch). Therefore, the difference in step responses remains relatively small. This is reflected by the diagram of Fig.7.12 showing the variation of the resulting relaxation length. Comparison with Fig.7.8 reveals that the relaxation lengths assessed for the responses to side slip (at small side slip) and camber have comparable magnitudes. This supports the theory of Eq.(7.11).

Comparison of the Figs.5.12 (lower left diagram) and 7.11a may reveal the quantitative difference in steady-state side force response to turn slip and camber angle. According to Eq.(3.55) the relationship between turn slip stiffness and camber stiffness will be:  $C_{F\gamma} = (1 - \varepsilon_\gamma)C_{F\varphi}/r_e$ . With the tyre effective rolling radius equal to approximately 0.3m and the estimated steady-state levels reached in Figs.5.12 and 7.11a for  $R = 115\text{m}$  and  $\gamma = 2^\circ$  respectively, we find for the reduction factor approximately:  $\varepsilon_\gamma = 0.5$ .

The response of the aligning torque to camber is similar to the response to turn slip (cf. Fig.5.12). The moment quickly reaches a maximum after which a slower decay to the steady-state level occurs. The string model with tread width effect predicts the same for the response to turn slip as can be concluded by adding the curves for  $M'_z$  and  $M_z^*$  (response to  $\varphi$ , Fig.5.10) in an appropriate proportion. The model developed in the present chapter generates a similar response but through a different mechanism. Equation (4.E71) that for  $F_x = 0$  takes the form

$$M_z = M'_z + M_{zr} = -t_\alpha F_y + M_{zr} \quad (7.40)$$

is used after having computed the transient slip and camber angles  $\alpha'$  and  $\gamma'$ .

As can be seen in Fig.4.13 or 4.21, the aligning torque caused by camber at zero slip angle is attributed to the residual torque  $M_{zr}$  and to the counteracting

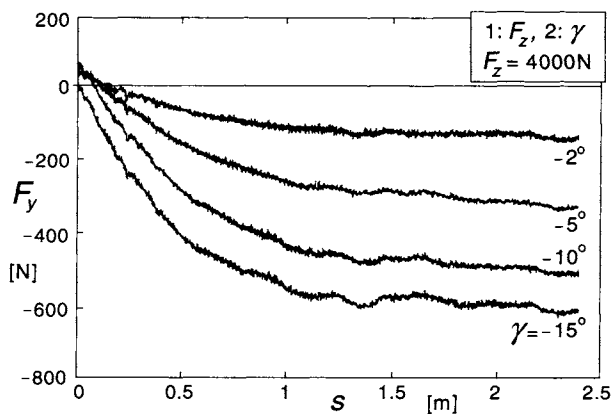


Fig. 7.11a. Side force response to step change in camber angle.

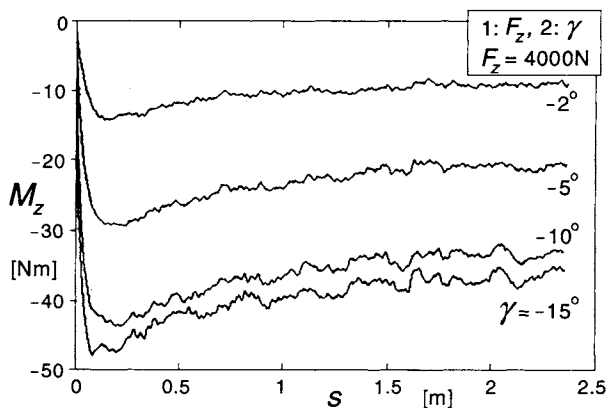


Fig. 7.11b. Moment response to step change in camber angle.

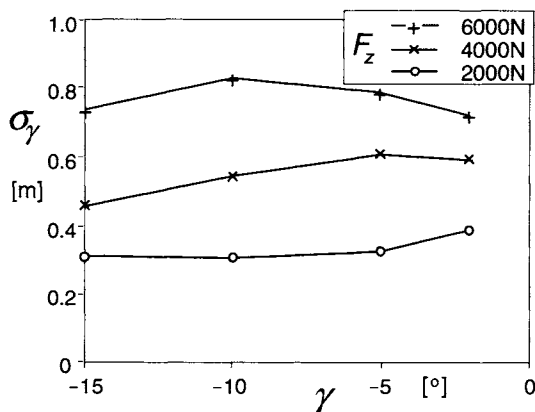


Fig. 7.12. Relaxation length for step responses to different camber angles (abscissa) at various wheel loads (camber after loading).



moment equal to the aligning stiffness  $C_{M\alpha}$  times  $\Delta\alpha_y$  which is the same as  $-t_\alpha F_y$  at  $\alpha = 0$ . The residual torque responds quickly with a relatively short relaxation length (about equal to half the contact length) or as has been suggested above for the present model: instantaneously. As the side force responds slowly with relaxation length  $\sigma_\alpha$ , and  $-t_\alpha F_y$  is opposite in sign with respect to the residual torque, a similar response as depicted in Fig.7.11b will be developed by the model represented by Eq.(7.40). The mechanism behind this response is supported by the physical reasoning that the moment due to tread width, that responds relatively fast to changes in camber and turn slip, gives rise to a yaw torsion of the carcass/belt in the contact zone which acts as a slip angle. This side slip generates a side force that acts in the same direction as the camber force generated by the camber induced spin. In addition, an aligning moment is generated that acts in a sense opposite to that of the tread-width camber (spin) moment. Ideally, in Fig.4.21, the moment due to camber spin is equal to the residual torque  $M_{zr}$  while  $-C_{M\alpha}\Delta\alpha_y = t_\alpha F_y$  is equal to the moment due to the yaw torsion induced side slip. However, in reality, only a part of the camber force  $F_y$  results from camber spin induced side slip. It is expected that the above analysis is partly true. Perhaps even for an appreciable part. The remaining part that is responsible for the 'hump' in the moment response must then be due to the transient asymmetric lateral tyre deformation that vanishes when the steady-state condition is reached. Figure 5.9 depicts the nature of this transient deflection.

In an alternative model, used for motorcycle dynamics studies dealing with possibly large camber angles, the other extreme is used and the term  $t_\alpha F_y$  is replaced by  $t_\alpha F_{y\alpha}$ , that is: with the side force attributed to the (transient) side slip angle alone (cf. Chapter 11).

#### 7.2.4. Non-Lagging Part

The force response to a change in camber exhibits a peculiar feature. From low velocity experiments conducted on the flat plank machine (cf. Fig.12.5), it turns out that directly after that the wheel is cambered (about the line of intersection), a side force is developed instantaneously. This, obviously, is caused by the non-symmetric distortion of the cross section of the lower part of the tyre. This initial 'non-lagging' side force that occurs at a distance rolled  $s=0$ , as shown in Fig. 7.11a, appears, for the tyre considered, to act in a direction opposite to the steady-state side force. Equal directions turn out to occur also: e.g. for a motorcycle tyre, cf. Segel and Wilson (1976). Also in these reported experiments, the camber angle is applied after the tyre has been loaded. Figure 7.13 gives the percentage of the non-lagging part with respect to the steady-state

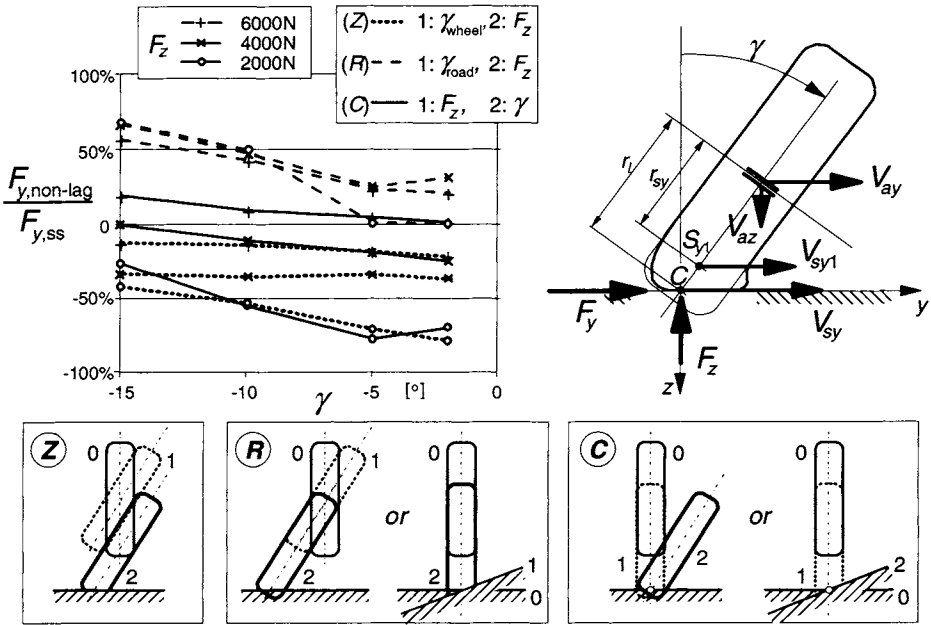


Fig. 7.13. Non-lagging part of side force response for the cases:

- (Z) loading the tyre vertically after having cambered the wheel,
- (R) loading the tyre radially after having cambered the wheel,
- or: loading the tyre vertically after having cambered the road,
- (C) applying wheel or road camber after having loaded the tyre.

Upper right diagram: New side slip point  $S_{y1}$  with side slip velocity component  $V_{sy1}$ .

side force for three wheel loads and for three different ways of reaching the loaded and cambered condition before rolling has started. In case (Z) the free wheel is first cambered and then loaded by moving it towards the horizontal road surface in vertical direction. This sequence appears to result in a somewhat larger non-lagging part. In the second case (R) the road surface is cambered first after which the tyre is loaded vertically. It turns out that now a response arises with the same sign as the steady-state response. The diagram indicates that also in case (C) the sign may remain unchanged if the wheel load is sufficiently high.

To simulate the development of the non-lagging side force, the following model is suggested. The tyre response that arises due to loading and/or tilting of the wheel while  $V_x = 0$ , is considered to be the result of the integrated lateral horizontal velocity of the lower part of the wheel. Beside the lateral velocity  $V_{sy}$  of the contact centre C, the lateral velocity  $V_{sy1}$  of a newly introduced slip point  $S_{y1}$  that is thought to be attached to the wheel at a radius  $r_{sy1}$  is used as an additional component of the effective lateral slip speed  $V_{sy,eff}$ . The upper right diagram of Fig.7.13 depicts the situation. We define:

$$V_{sy,eff} = \varepsilon_c V_{sy} + (1 - \varepsilon_c) V_{syl} \quad (\text{take } V_{sy,eff} = 0 \text{ if } F_z = 0) \quad (7.41)$$

with  $\varepsilon_c$  the participation factor. The effective lateral slip speed replaces  $V_{sy}$  in Eq.(7.7). In case of a horizontal flat road surface the velocities of the two points  $C$  and  $S_{yl}$  become:

$$V_{sy} = V_{ay} + \left( V_{az} \sin \gamma - r_l \frac{d\gamma}{dt} \right) \frac{1}{\cos \gamma} \quad (7.42a)$$

$$V_{syl} = V_{ay} - r_{sy} \frac{d\gamma}{dt} \cos \gamma \quad (7.42b)$$

The location of  $S_{yl}$  is defined through the proposed function for the slip radius:

$$r_{sy} = r_l - A_1 \frac{\rho_z}{\cos \gamma} \left( 1 - A_2 \sqrt{\frac{F_z}{F_{zo}}} - A_3 \gamma^2 \right) \quad (7.43)$$

The participation factor  $\varepsilon_c$  is defined by the proposed function:

$$\varepsilon_c = \frac{1 - A_4 |\gamma|}{1 + A_5 F_z / F_{zo} + A_6 (F_z / F_{zo})^2} \quad (7.44)$$

It may be seen from Eqs.(7.42a,b) that at constant camber angle and a purely vertical axle motion (case  $Z$ ),  $V_{syl} = V_{ay} = 0$ , and  $V_{sy} = V_{az} \tan \gamma$  is the governing component of the effective slip speed (7.41). If the loading is conducted by a radial approach of the road surface (case  $R$ ) we have  $V_{sy} = 0$ , and the governing part is  $V_{syl} = V_{ay} = -V_{az} \tan \gamma$ . The third case  $C$  is achieved by first vertical loading of the upright tyre,  $V_{sy} = V_{syl} = 0$ , and subsequently tilting the wheel about the line of intersection that is: about point  $C$ . In the latter phase the lateral slip velocity components become  $V_{sy} = 0$  and  $V_{syl} = (r_l - r_{sy})(d\gamma/dt) \cos \gamma$ .

For the tyre parameter values:  $C_{Fz} = 200 \text{ kN/m}$ ,  $C_{Fy} = 130 \text{ kN/m}$ ,  $F_{zo} = 4 \text{ kN}$ ,  $r_o = 0.3 \text{ m}$ ,  $r_c = 0.15 \text{ m}$ , and for Eqs.(4.E19-4.E30) with  $\zeta$ 's and  $\lambda$ 's = 1:  $p_{Cyl} = 1.3$ ,  $p_{Dyl} = 1$ ,  $p_{Eyl} = -1$ ,  $p_{Kyl} = 15$ ,  $p_{Ky2} = 1.5$ ,  $p_{Ky3} = 6$ ,  $p_{Ky4} = 2$ ,  $p_{Ky6} = 1$ ,  $p_{Vy3} = 1$  and remaining  $p$ 's = 0, the following values for  $A_1 \dots A_6$  were assessed through a manual fitting process:  $A_1 = 2.5$ ,  $A_2 = 0.8$ ,  $A_3 = 3$ ,  $A_4 = 2$ ,  $A_5 = -2.5$ ,  $A_6 = 10$ . With these values, the responses computed for the non-lagging part of the side force show reasonable correspondence with the experimental results of Fig.7.13.

The vertical load has been calculated using a tyre model with a circular contour of the cross section with radius  $r_c$ . For the more general case of an elliptic contour, cf. Fig.7.14, the following equations apply. We have for the coordinates of the lowest point:

$$\zeta = b / \sqrt{1 + \left( \frac{a}{b} \right)^2 \tan^2 \gamma}, \quad \eta = a \left( \frac{a}{b} \right) \tan \gamma / \sqrt{1 + \left( \frac{a}{b} \right)^2 \tan^2 \gamma} \quad (7.45)$$

The vertical compression  $\rho_c$ , which is the distance of the lowest point of the

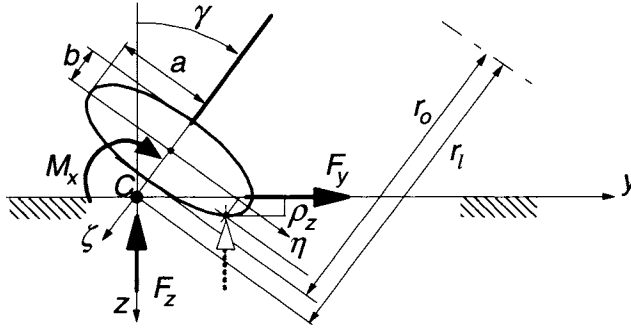


Fig. 7.14. Cross section contour with elliptical shape.

ellipse to the road surface if this distance is non-negative, now reads with  $r_o$  the free tyre radius and  $r_l$  the loaded tyre radius:

$$\rho_z = \max((r_o - r_l - b + \zeta) \cos \gamma + \eta \sin \gamma, 0) \quad (7.46)$$

In the simpler case of a circular contour ( $r_c = a = b$ ) the formula reduces to:

$$\rho_z = \max((r_o - r_l) \cos \gamma + r_c (1 - \cos \gamma), 0) \quad (7.47)$$

The normal load is now calculated as

$$F_z = C_{Fz} \rho_z \quad (7.48)$$

For a wheel subjected to oscillations, the observed tyre properties will be of importance especially when loss of road contact occurs. In Exercise 7.1 given at the end of this chapter and in Section 8.2, this problem is addressed. The more complex case of moving over short obstacles, exhibiting forward and transverse road slope variations, is treated in Section 10.1.6, Eqs.(10.35,10.36).

### 7.2.5. The Gyroscopic Couple

In Chapter 5 the gyroscopic couple that arises as a result of the time rate of change of the average tyre tilt deflection angle has been introduced. This angle is considered to be proportional with the lateral tyre deflection  $v$  or the side force  $F_y$ . Equation (5.178) may be written in terms of the deflection. With (5.179) and with the  $F_z/F_{zo}$  factor added to give smoother results for a jumping tyre, we get:

$$M_{z,gyr} = c_{gyr} m_t r_e \Omega \frac{dv}{dt} \frac{F_z}{F_{zo}} \quad (7.49)$$

where at free rolling the wheel speed of revolution equals the forward velocity divided by the effective rolling radius of the tyre. In general, we have:

$$\Omega = (V_x - V_{sx}) / r_e \quad (7.50)$$

For a radial ply steel-belted car tyre the non-dimensional coefficient  $c_{gyr}$  has been estimated to take the value 0.5. The quantity  $m_t$  represents the mass of the tyre. Extending the expression (7.40) yields for the total aligning moment:

$$M_z = M'_z + M_{zr} + M_{z,gyr} \quad (7.51)$$

### 7.3. Enhanced Non-Linear Transient Tyre Model

A totally different approach to model the transient rolling properties of the tyre is based on the separation of contact patch slip properties and carcass compliance not through the use of relaxation lengths but by incorporating the carcass springs in the model explicitly. The contact patch is given some inertia to facilitate the computational process (computational causality). This has the drawback that a relatively high natural frequency is introduced, possibly making the computation slower. We may, however, employ alternative methods to avoid the inclusion of the small mass. The model to be discussed, automatically accounts for the property that the lag in the response to wheel slip and load changes diminishes at higher levels of slip that in the previous section was realised by decreasing the relaxation length. This latter approach, however, appeared to possibly suffer from computational difficulties (at load variations). Also, combined slip was less easy to model. In developing the enhanced model, we should, however, try to maintain the nice feature of the relaxation length model to adequately handle the simulation at speeds near or equal to zero.

Figure 7.15 depicts the structure of the enhanced transient model. The contact patch can deflect in circumferential and lateral direction with respect to the lower part of the wheel rim. Only translations are allowed to ensure that the slip angle seen by the contact patch at steady state is equal to that of the wheel plane. To

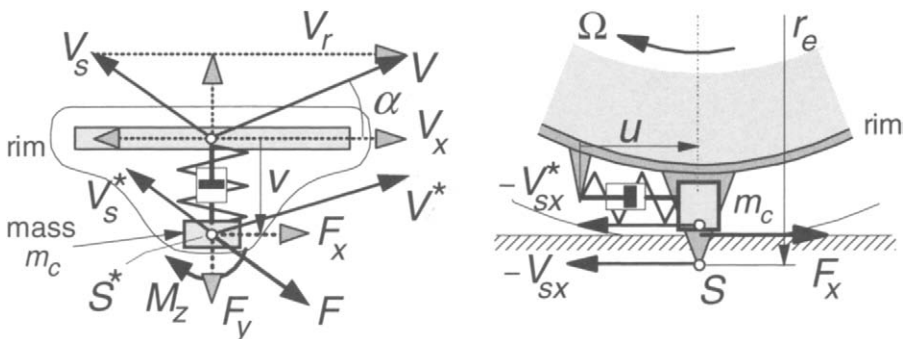


Fig. 7.15. Enhanced transient tyre model in top and side view showing carcass compliances and contact patch mass.

enable straightforward computations, a mass point is thought to be attached to the contact patch. That mass point coincides with point  $S^*$  the velocity of which constitutes the slip speed of the contact point. This slip velocity is used, together with the (assumedly at the contact patch detected) path curvature due to turn slip and wheel camber, to compute the forces  $F_x$ ,  $F_y$  and the moment  $M_z$  which act from road to contact patch. We may add a simple relaxation length model to enable computations near zero speed. The model was first employed by Van der Jagt et al. (1989) and later generalised by Pacejka and Besselink (1997). In Chapter 8 the model will be applied to investigate the effect of road undulations on the efficiency of anti-lock brake control.

With mass  $m_c$  and carcass stiffnesses  $c_{cx,y}$  and damping ratios  $k_{cx,y}$  introduced, the equations of motion for the contact patch mass point with longitudinal and lateral speed components  $V_{sx,y}^*$  read (yaw rate terms in accelerations disregarded):

$$m_c \dot{V}_{sx}^* + k_{cx} \dot{u} + c_{cx} u = F_x(\kappa', \alpha', F_z) \quad (7.52)$$

$$m_c \dot{V}_{sy}^* + k_{cy} \dot{v} + c_{cy} v = F_y(\alpha', \kappa', \gamma, F_z) - F_{y,NL} \quad (7.53)$$

The forces acting from ground to contact patch shown at the right-hand sides are computed from the steady-state formulae. The non-lagging camber force part  $F_{y,NL}$  is assumed to act directly on the wheel rim. We may approximate the non-lagging force part by a linear relation with  $\gamma$  using the camber thrust stiffness  $C_{Fy}$ , the non-lagging fraction  $\varepsilon_{NL}$  (cf. Sec.7.2.4) and the weighting function  $G_{y\kappa}$  (4.E59) to take care of the presence of a fore and aft force  $F_x$ :

$$F_{y,NL} = G_{y\kappa} \varepsilon_{NL} C_{Fy} \gamma \quad (7.54)$$

It is noted that  $\varepsilon_{NL}$  changes with  $F_z$  and  $\gamma$ , cf. Fig.7.13. For this reason we may better employ the method treated in Sec.7.2.4 with  $V_{sy,eff}$  replacing  $V_{sy}$  in (7.62).

To enable calculations near or at standstill we may add additional first-order differential equations with relaxation length  $\sigma_c$ . From these equations the transient slip quantities result which act as input in the steady-state slip force formulae. We have:

$$\sigma_c \frac{d\alpha'}{dt} + |V_x| \alpha' = -V_{sy}^* \quad (7.55)$$

$$\sigma_c \frac{d\kappa'}{dt} + |V_x| \kappa' = -V_{sx}^* \quad (7.56)$$

If needed, we may in the right-hand member of (7.53) replace argument  $\gamma$  with the transient spin slip  $\varphi'$  that results from an equation similar to (7.55):

$$\sigma_c \frac{d\varphi'}{dt} + |V_x| \varphi' = |V_x| \varphi \quad (7.57)$$

where in the right-hand member  $\varphi$  is to be replaced by the expression (7.13).

The contact relaxation length  $\sigma_c$  may be given a small but finite value, for instance equal to half the contact length,  $a_o$ , at nominal load that corresponds to our findings in Chapter 9. The equations (7.55-57) do not respond to load changes. For this, we rely on the effect of the carcass compliance (in conjunction with the load dependent cornering stiffness) which gives adequate results. Effectively, the resulting lateral compliance of the standing tyre is:

$$\frac{1}{C_{Fy}} = \frac{1}{c_{cy}} + \frac{\sigma_c}{C_{Fa}} \quad (7.58)$$

and the effective resulting tyre relaxation length (for side slip response):

$$\sigma_a = \frac{C_{Fa}}{C_{Fy}} = \frac{C_{Fa}}{c_{cy}} + \sigma_c \quad (7.59)$$

This equation may, in fact, be employed to assess the lateral carcass stiffness at ground level  $c_{cy}$ . From the measured tyre relaxation length  $\sigma_a$  and cornering stiffness  $C_{Fa}$  the lateral stiffness of the standing tyre  $C_{Fy}$  follows. By taking  $\sigma_c$  equal to half the contact length  $a$  the carcass lateral stiffness  $c_{cy}$  can be determined. The relaxation length for load variations remains equal to:

$$\sigma_{a,Fz} = \frac{C_{Fa}}{c_{cy}} \quad (7.60)$$

which is a little smaller than  $\sigma_a$ . Although this results from practical modelling considerations, we may in fact come close to the measurement results of Fig.7.10.

If one is not interested to include the ability to simulate near or at zero forward speed, the contact relaxation length  $\sigma_c$  may be disregarded and taken equal to zero. In Chapter 9 the contact relaxation length  $\sigma_c$  forms an essential element in the model developed for short wavelength behaviour.

The deflection rates needed in Eqs.(7.52,7.53) are equal to the difference in slip velocities:

$$\dot{u} = V_{sx}^* - V_{sx} \quad (7.61)$$

$$\dot{v} = V_{sy}^* - V_{sy} \quad (7.62)$$

As has been mentioned before, the wheel slip velocity  $V_s$  with components  $V_{sx,y}$  is defined as the horizontal velocity of the slip point  $S$  that is thought to be attached to the wheel rim a distance  $r_e$ , the effective rolling radius, below the wheel centre in the wheel centre plane.

$$V_{sx} = V_x - r_e \Omega \quad (7.63)$$

$$V_{sy} = V_y - r_e \dot{\gamma} \quad (7.64)$$

where  $V_{x,y}$  denote the horizontal (parallel to road plane) components of the wheel centre velocity. In Eq.(7.64) the camber angle is assumed to be small and  $r_e$  is replaced by the loaded radius  $r$ .

The forces acting on the wheel rim, finally, become:

$$F_{xa} = k_{cx} \dot{u} + c_{cx} u \quad (7.65)$$

$$F_{ya} = k_{cy} \dot{v} + c_{cy} v + F_{y,NL} \quad (7.66)$$

The aligning torque becomes:

$$M'_z = -t_a F_y \quad (7.67)$$

$$M_{zr} = M_{zr}(\gamma, \alpha', \kappa', F_z) \quad (7.68)$$

$$M_z = M'_z + M_{zr} + s \cdot F_x + M_{z,gyr} \quad (7.69)$$

The last equation forms an extension of Eq.(4.E71) through the introduction of the gyroscopic couple that follows from Eq.(7.49).

To illustrate the performance of the model, the calculated side force response to successive step changes in camber angle, slip angle and brake slip has been presented in Fig.7.16. The contact patch relaxation length  $\sigma_c$  has not been used in this example. In Chapter 8 the model is applied in the problems of controlled braking on an uneven road and on starting from standstill where in the latter case  $\sigma_c$  is employed. The less demanding case of the response of side force and aligning torque to successive steps in pure side slip, shown in Fig.7.17, was calculated with the transient model of Sec.7.2.3, Eq.(7.29). Very similar results are found when the enhanced model is used, that is: with the inclusion of carcass compliance and the contact mass  $m_c$ .

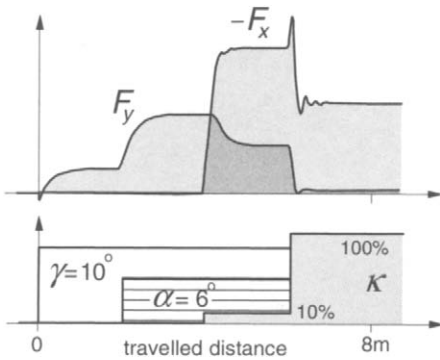


Fig. 7.16. Side force and brake force response to step changes in combined slip, computed with the enhanced transient tyre model of the present section.

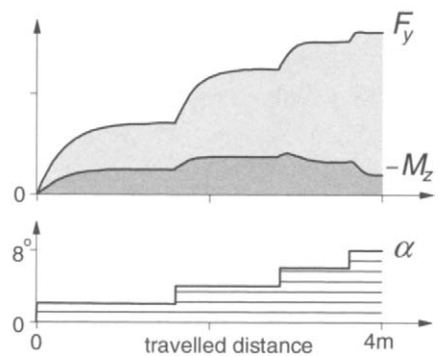


Fig. 7.17. Side force and aligning torque response to successive steps in side slip as computed with the transient fully non-linear model of Sec.7.2.4, Eq.(7.29).



### Exercise 7.1. Wheel subjected to camber, lateral and vertical axle oscillations

Consider the wheel assembly system depicted in Fig.7.18 the axle of which is constrained to move around a longitudinal hinge that is assumed to be positioned at a constant vertical height  $h$  above the smooth horizontal road surface. The hinge point moves forward in longitudinal direction with velocity  $V_x$ . This forward speed is assumed to increase linearly from zero at  $t = t_0$  until  $t = t_1$ , after which the speed remains  $V_x = V_{max}$ . The wheel axle is subjected to forced camber variation:

$$\gamma = \gamma_o + \hat{\gamma} \sin \omega t \quad (7.70)$$

Compute the response of the side force  $F_y$  by using the following equations:

$$\frac{dv_a}{dt} + \frac{1}{\sigma} V_x v_a = -V_{sy,eff} \quad (7.71)$$

$$\frac{dv_y}{dt} + \frac{1}{\sigma} V_x v_y = \frac{C_{Fy}}{C'_{Fa}} V_x \sin \gamma \quad (7.72)$$

where, protected against singularity:

$$\sigma = \max\left(\frac{C_{Fa}}{C_{Fy}}, 0.02\right) \quad (7.73)$$

and

$$C'_{Fa} = \max(C_{Fa}, 0.01) \quad (7.74)$$

Furthermore, the transient slip quantities, cf. (7.14,7.16), that replace  $\alpha^*$  and  $\gamma^*$  in Eqs.(4.E19-4.E30):

$$\alpha^* = \tan \alpha' = \frac{v_a}{\sigma}, \quad \gamma^* = \sin \gamma' = \frac{C_{Fa}}{C'_{Fy}} \frac{v_y}{\sigma} \quad (7.75)$$

with

$$C'_{Fy} = \max(C_{Fy}, 0.01) \quad (7.76)$$

Furthermore, use Eqs.(7.41-44,47,48) and for the side force Eqs.(4.E19-4.E30).

For the assembly and motion parameters we have:

$$e = 0.15 \text{ m}, f = 0.25 \text{ m}, h = 0.094 \text{ m}$$

$$t_0 = 0.1 \text{ s}, t_1 = 0.2 \text{ s}, t_{end} = 0.4 \text{ s}, V_{max} = 2, 5, 10 \text{ and } 20 \text{ m/s},$$

$$\gamma_o = 0.4 \text{ rad}, \hat{\gamma} = 0.12 \text{ rad}, \omega = 20\pi \text{ rad/s}$$

for the tyre parameters:

$$r_o = 0.3 \text{ m}, r_c = 0.05 \text{ m}, F_{zo} = 1000 \text{ N}, C_{Fz} = 60 \text{ kN/m}, C_{Fy} = 60 \text{ and } 120 \text{ kN/m},$$

and for Eqs.(4.E19-4.E30) with  $\zeta$ 's and  $\lambda$ 's = 1 and remaining  $p$ 's = 0:

$$p_{Cy1} = 1.3, p_{Dy1} = 1, p_{Ky1} = 10, p_{Ky2} = 1.5, p_{Ky4} = 2, p_{Ky6} = 1, \varepsilon_y = 0.01$$

and for Eqs.(7.43,44):

$$A_1 = 2.5, A_2 = 0.8, A_3 = 3, A_4 = 2, A_5 = -2.5, A_6 = 10.$$

Plot for the eight cases the computed  $F_y, F_z, \rho_z, \gamma, V_x$  and for comparison  $F_{y,st.}$  that arises if in Eqs.(4.E19-E30)  $\alpha^* = -V_{sy}/V_x$  and  $\gamma^* = \sin \gamma$  are used directly as input variables.

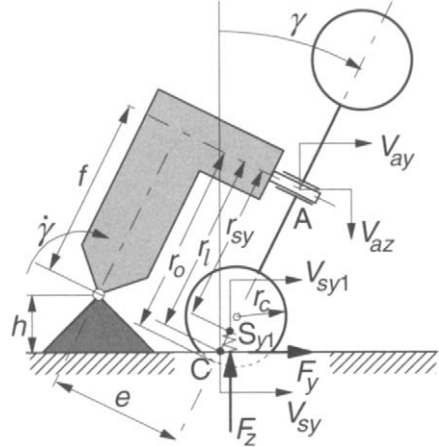


Fig.7.18. Rear view of wheel assembly subjected to combined camber, vertical and lateral oscillations (Exercise 7.1).